The microstructure and microwave dielectric properties of zirconium titanate ceramics in the solid solution system $ZrTiO_4$–$Zr_5Ti_7O_{24}$

C. L. WANG, H. Y. LEE, F. AZOUGH, R. FREER*
Manchester Materials Science Centre, University of Manchester/UMIST, Grosvenor Street, Manchester M1 7HS, UK

Zirconium titanate (ZT) ceramics having compositions in the range of $ZrTiO_4$–$Zr_5Ti_7O_{24}$ were prepared via the mixed oxide route, using ZnO and CuO as sintering aids and Y_2O_3 as stabilizer. Specimens were sintered at 1450 °C for 4 h and then cooled at 6 °C h^{-1}, 120 °C h^{-1} or air-quenched. All products exhibited densities exceeding 95% of the theoretical values. The amount of ZnO and CuO in the products decreased as the cooling rate decreased and as the content of TiO_2 increased. Energy dispersive analytical spectroscopy studies suggested that a grain boundary phase, rich in ZnO and CuO, existed as a continuous layer. Both composition and cooling rate were found to have significant effects on the microstructure of the zirconium titanate ceramics. Transmission electron microscopy showed that as the TiO_2 content increased, a superstructure with a tripled **a**-axis developed, but there was no obvious change in the lattice parameters. As the cooling rate decreased, extra peaks were observed in X-ray spectra and the lattice parameter in the **b** direction shortened dramatically; both are associated with cation ordering. A short-range commensurate superstructure with a $Z^{TT}ZZ^{TT}Z_{TT}ZZ_{TT}$ (or $Z_{TT}ZZ_{TT}Z^{TT}ZZ^{TT}$) stacking sequence was observed in the ordered $ZrTiO_4$ specimens. All the samples showed poor dielectric properties at microwave frequency (4 GHz). The low dielectric Q values (400–1000) were due to the presence of the structural stabilizer, Y_2O_3, within the grains. The Q value increased slightly with increasing TiO_2 content. The air-quenched samples had the highest Q values (850–1000); slower cooling led to the formation of microcracks within the samples and the reduction of Q values. The relative permittivity was controlled by bulk composition, the presence of a grain boundary phase, microcracks, oxygen vacancies and cation ordering. The ordering of cations and the presence of microcracks reduced the relative permittivity; rapidly cooled samples with higher TiO_2 content had higher relative permittivities (with a maximum of 44.3 for air-quenched $Zr_5Ti_7O_{24}$).

1. Introduction

The microwave frequency band is commonly considered to lie in the frequency range 0.9–300 GHz. In the last two decades, there has been a remarkable growth in microwave communications systems [1] and a wide range of dielectric materials have been developed for microwave applications [2–5].

Zirconium titanate-based ceramics have long been used in electronic applications where low-loss, temperature-stable dielectric materials are required [6]. Today, their applications also include resonator components in filters [7–9] and frequency-stable oscillators [10–12] at microwave frequencies. The end member $ZrTiO_4$ has an orthorhombic structure of α-PbO_2 type [13, 14] with space group of pbcn = D_{2h}^{14} [15]. The observed X-ray reflections obey the following extinction conditions, $0kl$: $k = 2n$, $h0l$: $l = 2n$, $hk0$: $h + k = 2n$. Coughanour *et al.* [16] noted that the **b** cell parameter of $ZrTiO_4$ quenched from temperatures above 1200 °C exhibited higher values than those for specimens quenched from lower temperatures, while the **a** and **c** cell parameters remained essentially the same. McHale and Roth [17] subsequently demonstrated that the **b** cell parameter of $ZrTiO_4$ depended sensitively on quench temperature and suggested that the change in the **b** cell parameter at about 1120 °C was associated with an order–disorder transformation; the latter proposal was confirmed by Bordet *et al.* [18] using powder neutron diffraction techniques. It is generally believed that the transition reflects the change from a disordered state at high temperature to one where there is certain degree of cation ordering at low temperature [19–24]. Recently, Christoffersen and Davies [25] employed high resolution transmission electron microscopy to study structures in the system $ZrTiO_4$–$Zr_5Ti_7O_{24}$, using single crystal fragments having variable composition. Their electron diffraction patterns revealed

0022–2461

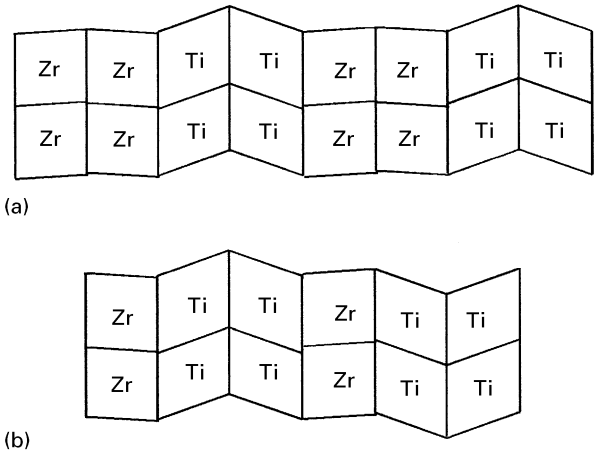

Figure 1 Schematic [0 1 0] projection of (a) ZZ^{TT} and (b) $Z^{TT}Z_{TT}$ cation stacking sequence.

that compositions with Zr:Ti between 1:1 and 5:7 had incommensurate superstructures; phases close to 1:1 were commensurate with a doubled **a**-axis superstructure and a ZZ^{TT} (or ZZ_{TT}) sequence of cation layers (Fig. 1a); phases close to 5:7 were also commensurate but with a tripled **a**-axis superstructure and a $Z^{TT}Z_{TT}$ sequence (Fig. 1b). The incommensurate, ordered zirconium titanates were found to be mixtures of two types of structural regions, one based on half multiples of $Z^{TT}Z_{TT}$ occupancy sequences, and the other based on integer multiples of ZZ^{TT} (or ZZ_{TT}) sequences.

The dielectric properties of $ZrTiO_4$ were first reported over five decades ago by Rath [6]. Within the past decade, the properties of $Zr_5Ti_7O_{24}$ and the effect of the phase transformation in $ZrTiO_4$ were investigated by Azough *et al.* [20, 26] and Christoffersen and Davies [25]. This study is concerned with the relationships between composition, microstructure and microwave dielectric properties of ceramics in the system of $ZrTiO_4$– $Zr_5Ti_7O_{24}$; five compositions were selected to span the full range. A small amount of Y_2O_3 was used to stabilize the low temperature structure and accelerate the order–disorder transformation [19].

2. Experimental procedure

2.1. Materials and preparation

Oxide powders of ZrO_2, TiO_2 (Tioxide A-HR Grade), ZnO (Analar Grade), CuO (Technical Grade) and Y_2O_3 (Analar Grade) were used as starting materials. Ceramic samples were prepared via the conventional mixed oxide route. The following compositions were chosen for the study:

1. ZT0: $ZrTiO_4$ + 1.0 wt % ZnO + 0.5 wt % CuO + 1.0 wt % Y_2O_3
2. ZT1: $ZrTi_{1.1}O_{4.2}$ + 1.0 wt % ZnO + 0.5 wt % CuO + 1.0 wt % Y_2O_3
3. ZT2: $ZrTi_{1.2}O_{4.4}$ + 1.0 wt % ZnO + 0.5 wt % CuO + 1.0 wt % Y_2O_3
4. ZT3: $ZrTi_{1.3}O_{4.6}$ + 1.0 wt % ZnO + 0.5 wt % CuO + 1.0 wt % Y_2O_3
5. ZT4: $ZrTi_{1.4}O_{4.8}$ ($Zr_5Ti_7O_{24}$) + 1.0 wt % ZnO + 0.5 wt % CuO + 1.0 wt % Y_2O_3

Oxides of the desired compositions were first ball-milled with propan-2-ol for 8 h, calcined at 1100 °C for 4 h and then milled again for 12 h. Pellets were pressed uniaxially at 120 MPa in the shape of rods with dimensions of 16 mm in diameter and 15 mm in thickness. The specimens were sintered at 1450 °C for 4 h in air and cooled at 6 °C h^{-1}, 120 °C h^{-1} or air-quenched.

2.2. Characterization of powders and products

The fired densities were determined from weight and dimension measurements. X-ray diffraction spectra were obtained by use of CuK_α radiation and a Philips horizontal X-ray diffractometer in connection with a Philips digital programmable controller (Model PW 1710) with a scanning interval of 0.05° in the range of 20–60° of 2θ. The lattice parameters were determined from computer-generated d-spacings of (0 2 0), (0 0 2), (2 0 0), (0 2 2), (2 2 0) and (2 0 2) reflections. As-fired surfaces and polished samples were examined by optical microscopy (Olympus, Model VANOX-T) and scanning electron microscopy (SEM Philips, Model 505 with energy dispersive spectroscopy (EDX) and Philips Model 525). Prior to the detailed optical examination, the specimens were ground on 1200 grade SiC paper, polished down to 1 μm diamond paste, then polished with OPS solution (Struers) and finally chemically etched at approximately 150 °C with concentrated sulphuric acid (98 vol % concentration) for 50 min. Average grain sizes were determined using the linear intercept method [27].

For transmission electron microscopy (TEM), samples cooled at 6 °C h^{-1} were crushed into grains, screened and ground again in an agate mortar and pestle. The final powders were then deposited on a carbon-coated copper grid. A Philips EM430 transmission electron microscope was used for lattice image and electron diffraction studies.

Microwave dielectric measurements were performed at 4 GHz on polished discs, approximately 12 mm diameter and 10 mm thick. The measurements were carried out at room temperature by use of the dielectric post method [28] with a Hewlett Packard vector analyser system (which comprised an 8757A scalar network analyser and an 8350B sweep oscillator).The relative permittivity and dielectric loss were obtained from the resonant frequency and the peak width of $TE_{0\,1\,1}$ resonant mode [29].

3. Results and discussion

Calcined powders of all compositions were white in colour. X-ray diffraction spectra showed they were mainly mixtures of monoclinic ZrO_2, tetragonal TiO_2 and a trace of orthorhombic TiO_2, indicating that the formation of the main zirconium titanate phase did not occur during calcining.

TABLE I The relative densities of the as sintered ZT ceramics

	Air-quenched	Cooling rate (%)	
		120 °C h^{-1}	6 °C h^{-1}
ZT0	95.8	96.4	95.4
ZT1	95.6	95.4	95.8
ZT2	96.2	95.5	95.3
ZT3	95.5	95.0	94.8
ZT4	95.3	95.3	95.1

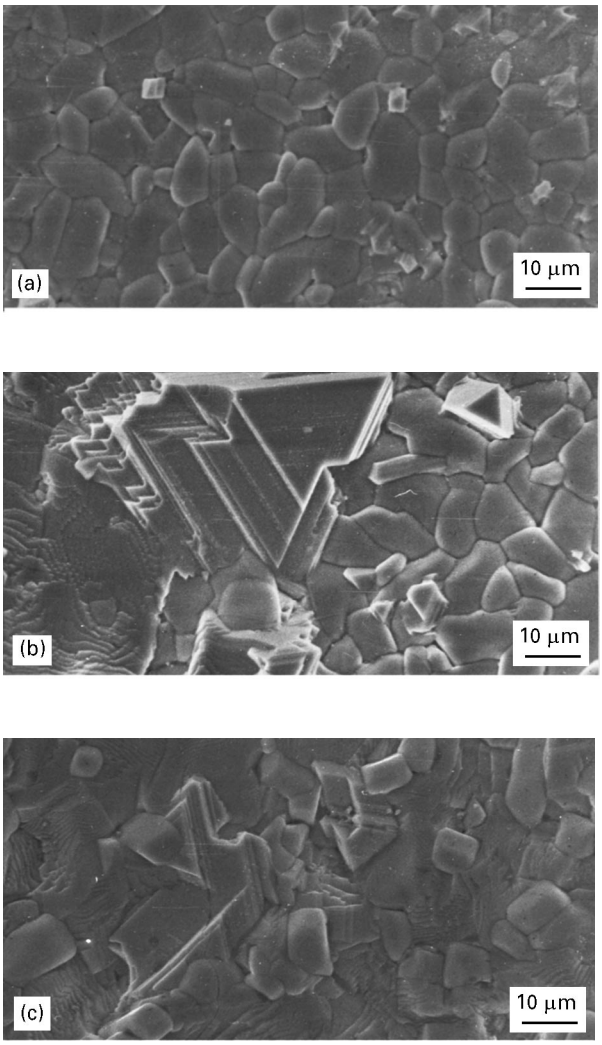

Figure 2 SEM micrographs of (a) ZTO, (b) ZT2 and (c) ZT4 cooled at 6 °C h^{-1}, showing the amount of the second phase (large triangular grains) increased as the TiO_2 content increased.

3.1. Microstructure development

All the sintered ceramics, except the slowly cooled ZT3, had relative densities over 95% of the theoretical value (Table I). Neither composition nor cooling rate had any significant effect on specimen density. The as-sintered ceramics were brown in colour due to the addition of CuO. The slowly cooled (6 °C h^{-1}) samples were lighter in colour than the air-quenched samples. Since both ZnO and CuO are volatile, and the slowly cooled samples spent extended periods at elevated temperatures, the changes in colour reflect the decreasing amounts of ZnO and CuO remaining in the samples as the cooling rate decreased.

TABLE II The composition of the second phase of ZT ceramics

Oxide	ZrO_2	TiO_2	ZnO	CuO
Wt %	3	31	42	24

TABLE III The average grain sizes of ZT ceramics cooled at various rates

Cooling rate	Grain size (μm)
Air-quenched	4.7 ± 0.5
120 °C h^{-1}	5.3 ± 0.7
6 °C h^{-1}	7.2 ± 0.7

Second phases, several microns in size, were observed on the as-fired surfaces. The amount of second phase increased as the TiO_2 content increased (Fig. 2) and was independent of the cooling rate. EDX analyses showed the second phase was rich in ZnO, CuO and TiO_2 with a small amount of ZrO_2 (Table II). On polished and etched surfaces, the large second phase grains were not observed; the additives ZnO and CuO were not detected within the primary grains but in the thin grain boundary phase. The results infer that the ZnO and CuO contents of the grain boundary phase decreased with increasing TiO_2 content for the samples cooled at the same rate, and that the grain boundary phase existed as a continuous layer.

The average grain size of the samples depended on the cooling rate, but was independent of composition. Grain size increased as the cooling rate decreased (Table III) because the more slowly cooled samples were effectively subjected to longer sintering times. Samples cooled at 6 °C h^{-1} have grain sizes ~50% larger than air-quenched specimens. The microstructures of the ZT ceramics were sensitive to the heat treatment conditions and composition. Fig. 3 shows, for example, optical micrographs of ZT0 samples which had been (i) air-quenched and (ii) cooled at 6 °C h^{-1}. In the air-quenched samples, grains were rounded, crack-free and of uniform size (Fig. 3a). As the cooling rate decreased, the grains became distorted and microcracks developed (Fig. 3b). The amount of cracks increased significantly as the cooling rate decreased. For samples cooled at the same rate, e.g. 120 °C h^{-1} (Fig. 4), the microstructure changed as TiO_2 content increased; the amount of microcracks initially increased and then decreased and the pores became more aggregated.

Fig. 5 shows X-ray diffraction spectra of ZT0 cooled at various rates. As the cooling rate was decreased, a broad extra peak appeared (indicated by *); this was accompanied by a decrease in the intensity of the neighbouring (1 1 0) reflection, indicating the development of cation ordering within the structure. X-ray diffraction spectra of the slowly cooled samples (6 °C h^{-1}) are shown in Fig. 6. The (2 1 1) superstructure reflection appeared in ZT2, ZT3 and ZT4, indicating that they had a commensurate superstructure with a tripled **a**-axis. For the air-quenched samples

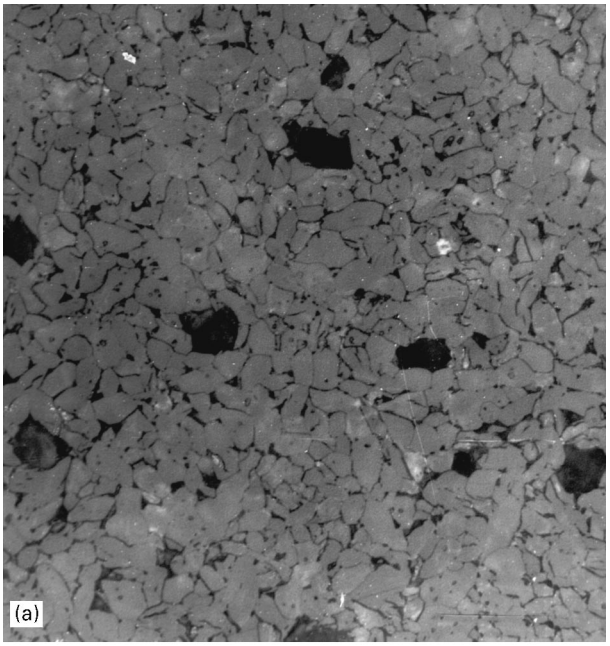

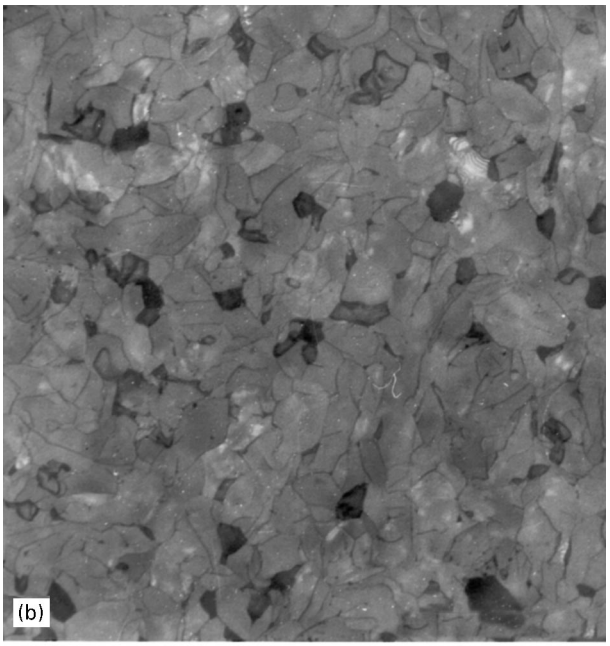

Figure 3 Optical micrographs of ZT0 ceramics: (a) air-quenched; (b) cooled at 6 °C h^{-1}. Scale bars = 40 μm.

(Fig. 7), the superstructure reflection (indicated by *) was also observed in ZT2, ZT3 and ZT4, inferring a certain degree of ordering in the rapidly cooled ZT2, ZT3 and ZT4 samples.

Lattice parameters were affected mainly by the cooling rate. There was no significant change in the lattice parameters with the composition, but a slight increase in lattice parameter in the **b** direction of air-quenched specimens was noted (Fig. 8). The lengths of the lattice parameter in the **a** direction and lattice parameter in the **c** direction were essentially unchanged with the cooling rate, approximately 0.48 nm and 0.50 nm, respectively, for all the specimens (Fig. 8). The lengths of lattice parameter in the **b** direction decreased in a remarkable way as the

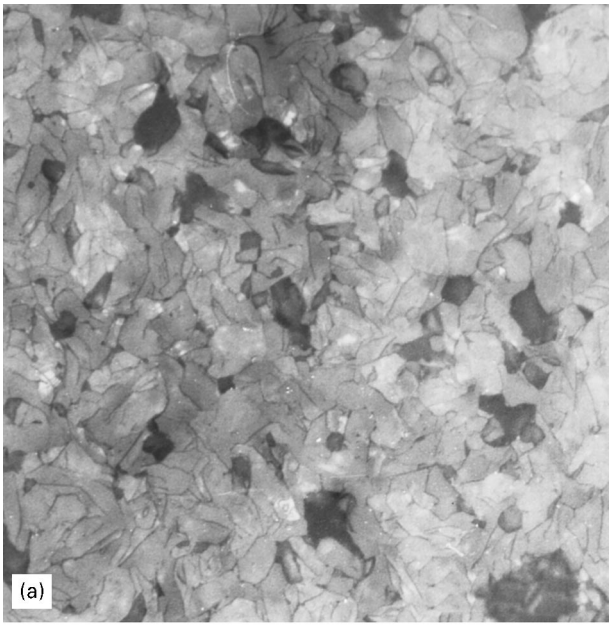

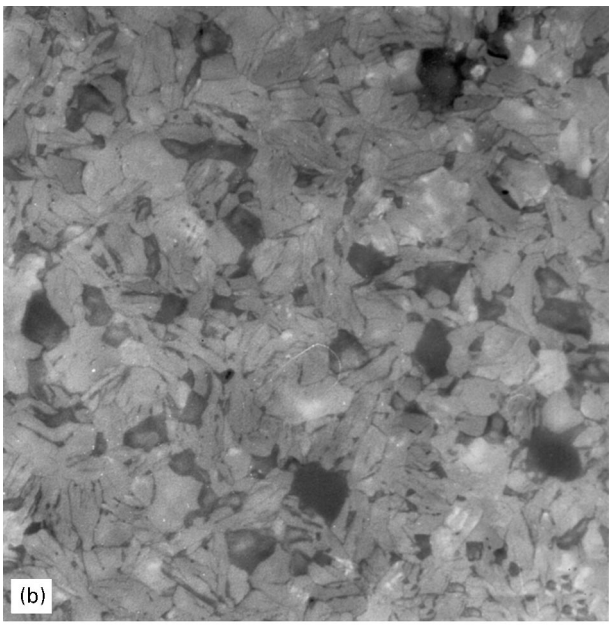

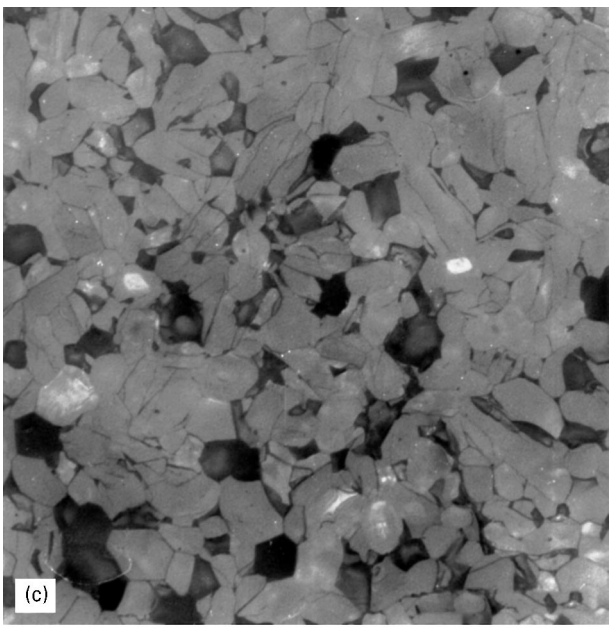

Figure 4 Optical micrographs of ZT ceramics cooled at 120 °C h^{-1}: (a) ZT0; (b) ZT2; (c) ZT4. Scale bars = 40 μm.

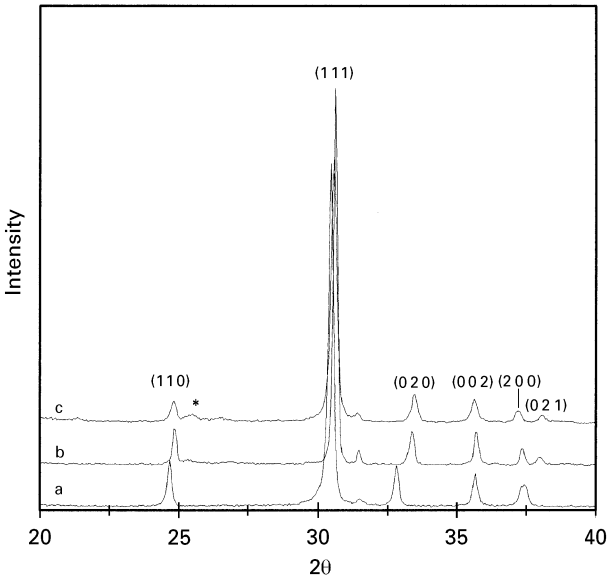

Figure 5 X-ray diffraction spectra for ZT0 samples cooled at various rates: (a) air-quenched; (b) 120 °C h^{-1}; (c) 6 °C h^{-1} (see text for explanation).

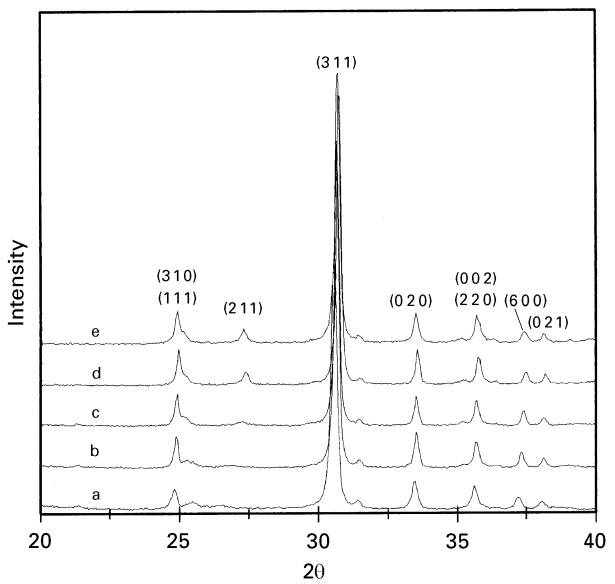

Figure 6 X-ray diffraction spectra for samples cooled at 6 °C h^{-1}: (a) ZT0; (b) ZT1; (c) ZT2; (d) ZT3; (e) ZT4.

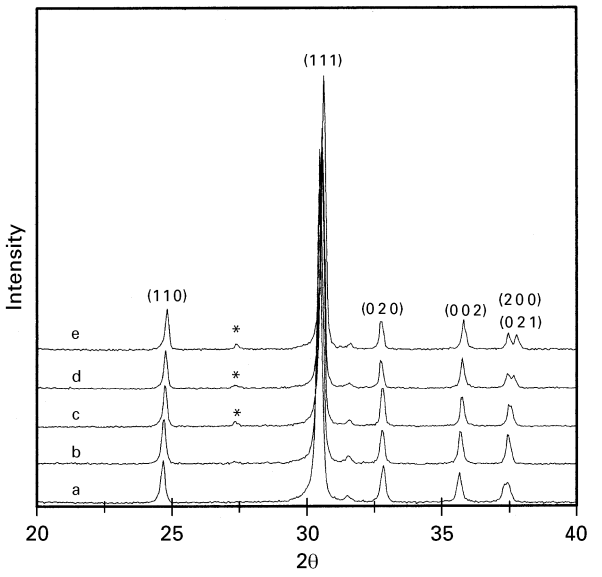

Figure 7 X-ray diffraction spectra for air-quenched samples: (a) ZT0; (b) ZT1; (c) ZT2; (d) ZT3; (e) ZT4.

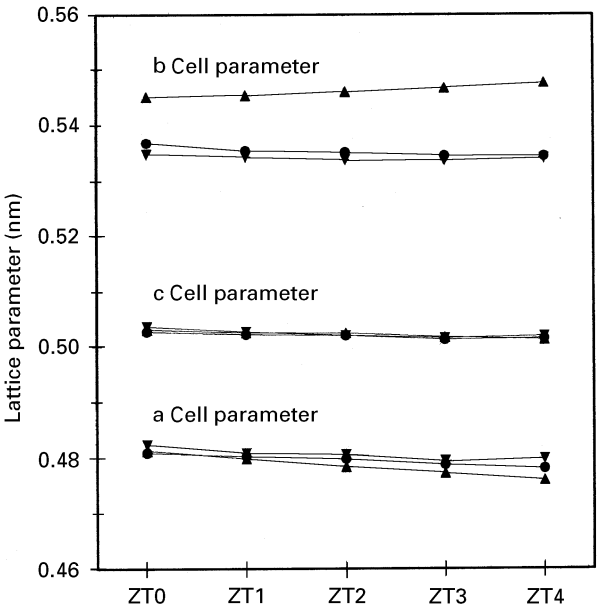

Figure 8 Lattice parameter as a function of composition for ZT ceramics (▲ air quenched; ● cooled at 120 °C h^{-1}; ▼ cooled at 6 °C h^{-1}).

cooling rate decreased (Fig. 9), due to the order–disorder transformation [19].

The slowly cooled samples were examined in detail by TEM. Fig. 10 illustrates schematically the [0 1 0] electron diffraction pattern of the incommensurate ordered structure of ZT ceramics. Three types of diffraction spots were observed (fundamental reflections, first-order satellite reflections and second-order satellite reflections). The indices of the satellite reflections, (h_s k_s l_s), can be given by

$$h_s = h_0 \pm m\alpha, \qquad k_s = k_0, \qquad l_s = l_0$$

where h_0, k_0 and l_0 are indices of the fundamental reflections, m is the order of the satellite reflections, and α is the distance from a satellite reflection to its

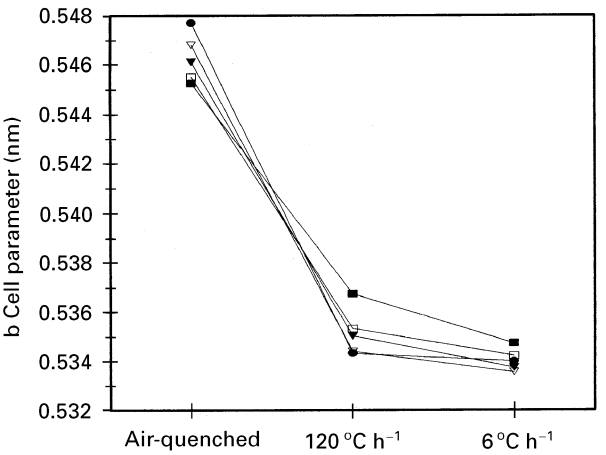

Figure 9 Lattice parameter in the **b** direction as a function of the cooling rate for ZT ceramics (■ ZT0; □ ZT1; ▼ ZT2; ▽ ZT3; ● ZT4).

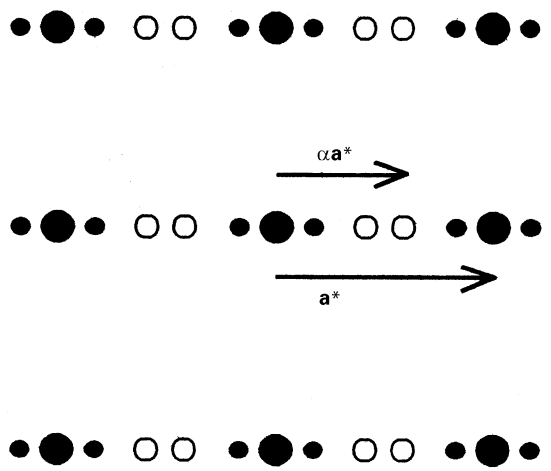

Figure 10 Schematic [0 1 0] electron diffraction pattern of the incommensurate ordered structure of ZT ceramics (● fundamental reflections; ○ first-order satellite reflections; ● second-order satellite reflections).

corresponding fundamental reflection in terms of a fraction of the length of **a*** (Fig. 10). Fig. 11 shows [0 1 0] electron diffraction patterns for ZT0, ZT1 and ZT2 cooled at 6 °C h^{-1}. The incommensurate form of ordered ZT0 is characterized by the presence of satellite reflection spots at non-integral positions on either side of the fundamental reflections (Fig. 11a). The satellite reflections also exhibited a varying degree of continuous streaking in the **a** direction. For ZT1 (Fig. 11b), the separation of the first-order satellite reflections was greater and the second-order satellite reflections were further from the fundamental reflections (than in ZT0), reflecting a change in the stacking sequence. The electron diffraction pattern of ZT2 (Fig. 11c) shows a commensurate superstructure with a tripled **a**-axis. The streaking along the **a** direction indicates that the superstructure was not fully formed. The results confirm that ZT0 and ZT1 had incommensurate ordered structures, while ZT2, ZT3 and ZT4 had commensurate superstructures with a tripled **a**-axis. This substantiates the trends indicated by the X-ray diffraction results (Fig. 6). The commensurate superstructures appear to exist in a wider composition range than that observed by Christoffersen and Davies [25].

Fig. 12 is an [0 1 0] TEM bright field image of ZT0 cooled at 6 °C h^{-1}; Zr layers are shown by the dark bands, while Ti layers are the brighter bands. The ZTT (Z^{TT} or Z_{TT}) and ZZTT (ZZ^{TT} or ZZ_{TT}) slabs, reported by Christoffersen *et al.* [25], were found to be representative of the structure as a whole. An abrupt change in occupancy of cation layers from more Zr-rich to more Ti-rich, or vice versa, is indicated by arrows in Fig. 12. A short-range stacking sequence of ZTTZZTT ($Z^{TT}ZZ^{TT}$ or $Z_{TT}ZZ_{TT}$), which has not been previously reported, was observed; this stacking sequence was distributed throughout the structure.

The ZZTT stacking unit can be formed from a ZTT-type structure by the insertion of a planar fault with a displacement of $-(1/3)\mathbf{a}_{ord}$ (where $\mathbf{a}_{ord}$ is the length of lattice parameter in the **a** direction of ordered $Zr_5Ti_7O_{24}$). Christoffersen and Davies [25]

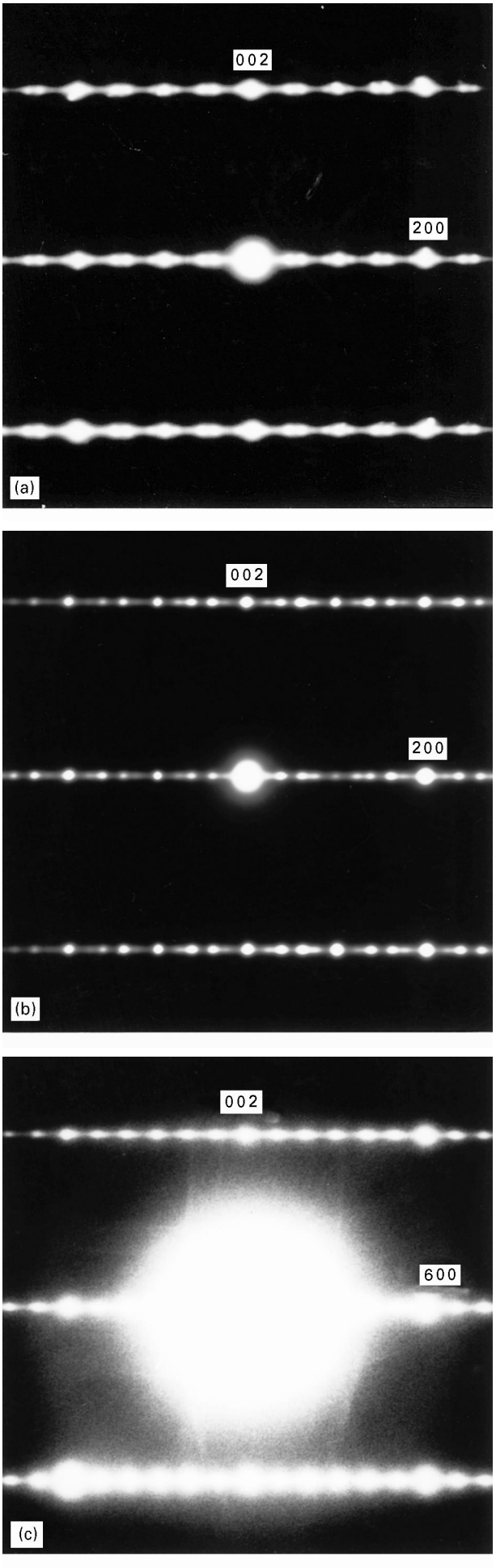

Figure 11 [0 1 0] electron diffraction patterns of specimens cooled at 6 °C h^{-1}: (a) ZT0, (b) ZT1 and (c) ZT2.

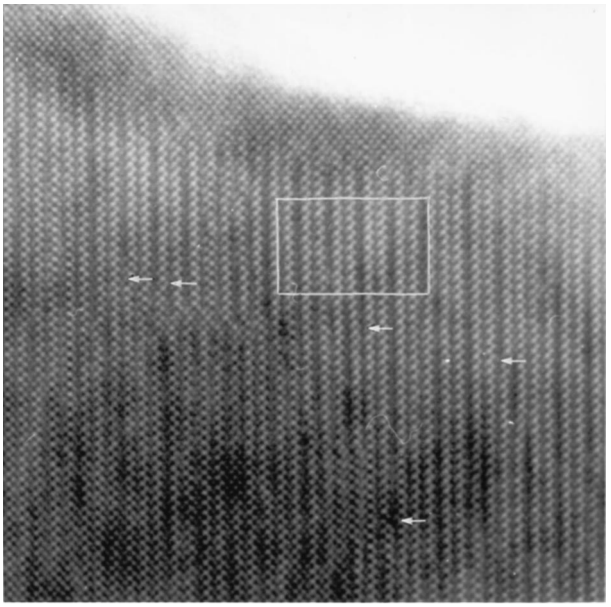

Figure 12 [0 0 1] TEM bright field image of ZT0 specimen cooled at 6 °C h^{-1}. Arrows indicate abrupt change of occupancy between Zr-rich and Ti-rich layers. Box indicates ZTTZZTT stacking sequence (see text).

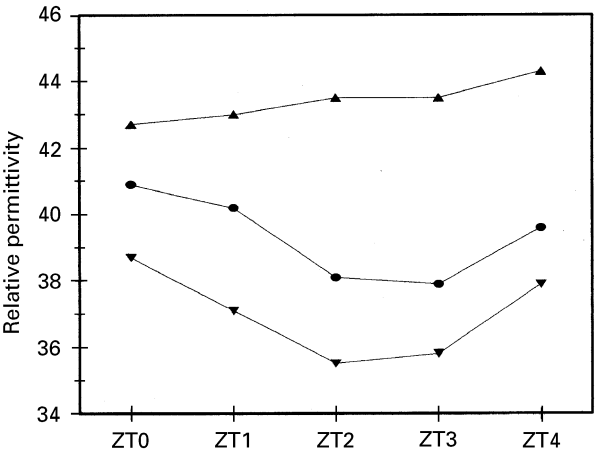

Figure 13 Relative permittivity (at 4 GHz) as a function of composition for ZT ceramics (▲ air quenched; ● cooled at 120 °C h^{-1}; ▼ cooled at 6 °C h^{-1}). All relative permittivity values are reliable to ± 0.3.

have shown that the non-integral satellite reflections arise not from any modulation within ZTT and ZZTT regions, but from the fact that the ZZTT regions are the result of antiphase boundaries within the ZTT structure, and that the modulation wavelength, L, can be determined by

$$L = 1/\alpha = 3M/(2M - 1)$$

where M is the average fault spacing in multiples of $\mathbf{a}_{dis}$ (the length of lattice parameter in the **a** direction of disordered $ZrTiO_4$). The modulation wavelengths calculated from the electron diffraction pattern (Fig. 11a) and the bright field image (Fig. 12) are 1.74 ($\alpha = 0.575$) and 1.72 ($M = 3.91$), respectively, and that for an entire ZTTZZTT ($Z^{TT}ZZ^{TT}Z_{TT}ZZ^{TT}$) structure is 1.75 ($M = 3.5$). The three data are in good agreement. A region consisting of a ZTTZZTT sequence in the lattice image is outlined in Fig. 12. The previously reported entire ZZTT slab [25] was, however, not detected in the present study.

3.2. Microwave dielectric properties

The microwave dielectric properties were measured at 4 GHz. All ZT ceramics showed poor dielectric properties at microwave frequency due to the presence of Y_2O_3 in the primary grains, as noted by Azough *et al.* [26] for $Zr_5Ti_7O_{24}$. Unfortunately, Y_2O_3 appears to be necessary to stabilize the structures of the TiO_2-rich compositions.

The presence of second phases and microcracks, variation in sintered density (porosity), defects and order-disorder transformations are believed to be the main factors which affect the relative permittivity. For a multi-phase ceramic, the overall relative permittivity can be predicted from the volume fraction and the relative permittivity of each component by the logarithmic mixture rule [30]

$$\log \varepsilon_r = \Sigma V_i \log \varepsilon_i$$

where ε_r is the overall relative permittivity, and V_i and ε_i are the volume fraction and the relative permittivity of the component i, respectively. In the present work, the theoretical densities of all ZT ceramics are of same magnitude, therefore the degradation of the relative permittivity caused by the porosity is approximately the same for all the samples. The effects of second phases can be neglected since the volume fraction is small compared to the whole.

Fig. 13 shows the relative permittivity as a function of the composition. For the air-quenched samples, the relative permittivities increased slightly with increasing the TiO_2 content. For samples cooled at 120 °C h^{-1} and 6 °C h^{-1}, the relative permittivities at first decreased then increased with increasing TiO_2 content. Since the microcracks developed in the structure due to the lattice contraction at lower cooling rates, and the amount of cracks was greatest in ZT2 and ZT3 (mid range TiO_2 content) (see Fig. 4); the results suggest that the microcracks have a significant effect on the relative permittivity of samples cooled at 120 °C h^{-1} and 6 °C h^{-1}. However, in the crack-free samples (air-quenched samples), the results show that the relative permittivity was higher in samples with higher TiO_2 contents.

Fig. 14 shows the relative permittivity of ZT ceramics as a function of cooling rate. A steady decrease in the relative permittivity with reduction of the cooling rate was observed. The results are consistent with the findings of Christoffersen *et al.* [24]. It was reported by Christoffersen *et al.* [24] for $ZrTiO_4$ and by Hirano *et al.* [31] for (Zr, Sn)TiO_4, that the contraction in the lattice parameter in **b** direction due to the order–disorder transformation led to a reduction in the ionic polarization and in turn to a reduction in the relative permittivity. The present results for $ZrTiO_4$–$Zr_5Ti_7O_{24}$ ceramics (Fig. 14) confirm this trend.

The Q value may be affected by second phase, porosity, microcracks, defects and order–disorder transformations [20]. In the present study, the grain

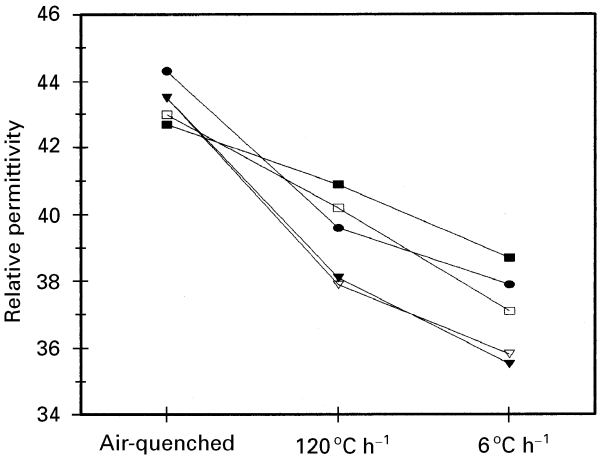

Figure 14 Relative permittivity (at 4 GHz) of ZT ceramics as a function of the cooling rate (■ ZT0; □ ZT1; ▼ ZT2; ▽ ZT3; ● ZT4).

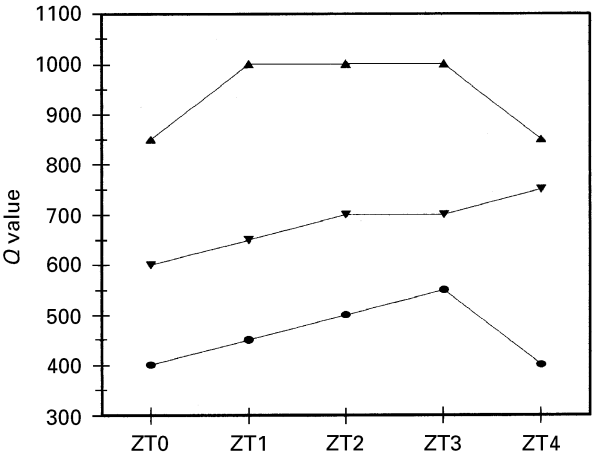

Figure 15 Dielectric Q value (at 4 GHz) of ZT ceramics as a function of the composition (▲ air quenched; ● cooled at 120 °C h^{-1}; ▼ cooled at 6 °C h^{-1}). All Q values are reliable to $\pm$ 50.

boundary phase was rich in ZnO, CuO and TiO_2 and has a low Q value [20]. The loss of this (Zn–Cu–Ti)-rich boundary phase during sintering from the more slowly cooled samples should improve the Q value slightly. Pores will generally degrade the Q value, but Hirano *et al.* [31] noted that the Q value was independent of the density in the range of 90–98% theoretical density. Therefore, pores should not have a significant influence in the present study. The reduction in the Q value caused by microcracks was acknowledged by O'Bryan *et al.* [32] for $BaTi_4O_9$ and $Ba_2Ti_9O_{20}$; a reduction of at least 40% in the Q value was observed. Microcracks are also expected to reduce the Q value of these ZT ceramics.

In complex perovskites, the Q values tend to increase when cations become more ordered. In the studies of $Ba(Zn_{1/3}\ Ta_{2/3})O_3$ [4, 33], the Zn–Ta ordering increased the Q value by as much as a factor of 10. This increase in the Q value was believed to be the result of the decrease in the lattice strain associated with segregating the two cations. However, zirconium titanate ceramics do not appear to behave in the same way because a decrease in the Q value with increasing the cation ordering has also been reported for ZT ceramics [24].

Figs 15 and 16 illustrate the variation of Q value with composition and the cooling rate respectively. The highest Q value (1000) was obtained for air-quenched samples and the lowest Q values (400) were obtained with samples cooled at 120 °C h^{-1}. For samples cooled at 6 °C h^{-1}, an increase in the Q value for all compositions was noted (Fig. 15). However, Q values seemed to be independent of the composition. The variation of Q value with cooling rate was unusual for all compositions (Fig. 16). There was a remarkable fall from 1000 to 400 between the air-quenched samples and those cooled at 120 °C h^{-1} due to the introduction of microcracks in the lattice. As the cooling was further decreased, the Q value increased, possibly due to the effects of ordering [3, 33], or more likely the elimination of oxygen vacancies [31, 34]. However, the Q values depend critically on the processing conditions, and the resulting cleanliness of the grains and grain boundaries.

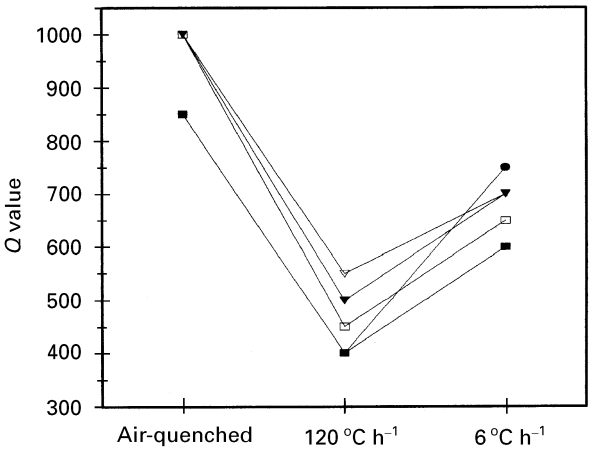

Figure 16 Dielectric Q value (at 4 GHz) of ZT ceramics as a function of the cooling rate (■ ZT0; □ ZT1; ▼ ZT2; ▽ ZT3; ● ZT4).

4. Conclusions

1. Mixed oxide prepared ceramics in the system $ZrTiO_4$–$Zr_5Ti_7O_{24}$ were of $\sim$ 95% theoretical density with grain sizes of 4.7–7.2 μm.

2. The additives ZnO and CuO were found in a thin grain boundary phase; the amount of ZnO and CuO decreased as the cooling rate decreased and the TiO_2 content increased.

3. For all compositions the length of the lattice parameter in the **b** direction fell dramatically from 0.546 nm to $\sim$0.535 nm as the cooling rate after sintering was reduced, reflecting ordering of the cations.

4. TEM studies showed the existence of commensurate superstructures with a tripled **a**-axis over a wide composition range (ZT2, ZT3 and ZT4). A new stacking sequence of ZTTZZTT was observed in the low temperature ordered form of $ZrTiO_4$.

5. In rapidly cooled samples the relative permittivity of the samples increased slightly with increasing TiO_2 content; for specimens cooled more slowly, the relative permittivity was lower (particularly in ZT2 and ZT3), because of cation ordering and the presence of microcracks.

6. Dielectric Q values at 4 GHz were low for all specimens (400–1000) due to the presence of the

stabilizer Y_2O_3 in the primary grains. The highest Q values (850–1000) were obtained for the rapidly cooled specimens. In general, the Q value increased with TiO_2 content up to ZT3 ($ZrTi_{1.3}O_{4.6}$); but slower cooling, causing cation ordering and the presence of microcracks, reduced the Q values.

References

1. T. NEGAS, G. YEAGER, S. BELL and N. COATS, *Amer. Ceram. Soc. Bull.* **72** (1993) 80.
2. H. M. O'BRYAN, J. THOMSON and J. K. PLOURDE, *ibid.* **57** (1974) 450.
3. S. NOMURA, K. TOYAMA and K. KANETA, *Jpn. J. Appl. Phys.* **21** (1982) L-624.
4. S. KAWASHIMA, M. NISHIDA, I. UEDA and H. OUCHI, *J. Amer. Ceram. Soc.* **66** (1983) 421.
5. K. WAKINO, K. MINAI and H. TAMURA, *ibid.* **67** (1984) 278.
6. W. RATH, *Keram. Radsch.* **49** (1941) 137.
7. K. WAKINO, T. NISHIKAWA, S. TAMURA and Y. ISHIKAWA, in Proceedings of the 1975 IEEE Microwave Theory Technical Symposium, p. 63 (Institute Electrical and Electronic Engineers (IEEE), USA). (1975).
8. K. WAKINO, T. NISHIKAWA, H. MATSUMOTO and Y. ISHIKAWA, in Proceedings of the 1978 IEEE Microwave Theory Technical Symposium, p. 230 (Institute Electrical and Electronic Engineers (IEEE), USA). (1978).
9. M. W. POSPIESZALSKI, *IEEE Trans. Microwave Theory Tech.* **MTT-27** (1979) 233.
10. K. HIRAI, T. OKIKAWA and N. AIBA, *Toshiba Rev.* **115** (1978) 37.
11. T. SAITO, Y. ARAI, H. KAMZIZO, Y. ITOH and T. NISHIKAWA, in Proceedings of the 1979 IEEE Microwave Theory Technical Symposium, p. 197 (Institute Electrical and Electronic Engineers (IEEE), USA). (1979).
12. O. ISHIHARA, T. MORI, H. SAWANO and M. NAKATANI, *IEEE Trans. Microwave Theory Tech.* **MTT-28** (1980) 817.
13. G. BLASSE, *Z. Anorg. Allg.* **345** (1966) 225.
14. R. W. LYNCH and B. MOROSIN, *J. Amer. Ceram. Soc.* **55** (1972) 409.
15. R. E. NEWNHAM, *ibid.* **50** (1967) 216.
16. L. W. COUGHANOUR, R. S. ROTH and V. A. DEPROSSE, *J. Res. Nat. Bur. Stand.* **52** (1954) 37.
17. A. E. McHALE and R. S. ROTH, *J. Amer. Ceram. Soc.* **66** (1983) C-18.
18. P. BORDET, A. E. McHALE, A. SANTARO and R. S. ROTH, *J. Solid State Chem.* **64** (1980) 30.
19. A. E. McHALE and R. S. ROTH, *J. Amer. Ceram. Soc.* **69** (1986) 827.
20. F. AZOUGH, Ph.D Thesis, University of Manchester, Manchester, UK (1991).
21. T. YAMADA, K. URABE, H. IKAWA and H. SHIMOJIMA, *J. Ceram. Soc. Japan* **99** (1991) 380.
22. A. YAMAMOTO, K. TANAKA, H. MARUMO and HUKUNAGA, *Acta Crystallogr* **47C** (1991) 1588.
23. R. CHRISTOFFERSEN and P. K. DAVIES, *Solid State Ionics* **57** (1992) 59.
24. R. CHRISTOFFERSEN, P. K. DAVIES and X. WEI, *J. Amer. Ceram. Soc.* **77** (1994) 1441.
25. R. CHRISTOFFERSEN and P. K. DAVIES, *ibid.* **75** (1992) 563.
26. F. AZOUGH, A. WRIGHT and R. FREER, *J. Solid State Chem.* **108** (1994) 284.
27. M. I. MENDELSON, *J. Amer. Ceram. Soc.* **52** (1969) 443.
28. B. W. HAKKI and P. D. COLEMAN, *IRE Trans Microwave Theory Tech* **MTT-8** (1960) 402.
29. D. HENNINGS and H. SCHNABEL, *Philips J. Res.* **38** (1983) 295.
30. K. LICHTENECKER, *Phys. Z.* **10** (1909) 1005.
31. S. I. HIRANO, T. HAYASHI and A. HATTORI, *J. Amer. Ceram. Soc.* **74** (1991) 1320.
32. H. M. O'BRYAN, J. THOMSON and J. K. PLOURDE, *Ber Dt. Keram, Ges.* **55** (1978) 348.
33. K. MATSUMOTO, T. HIUGA, K. TAKADA and H. ICHIMURA, in Proceedings of the Sixth IEEE International Symposium on Applications of Ferroelectrics, USA (1986) p. 118.
34. N. MICHIURA, T. TATEKAWA, Y. HIGUCHI and H. TAMURA, *J. Amer. Ceram. Soc.* **78** (1995) 793.

Received 28 June
and accepted 31 July 1996